A solute-binding protein in the closed conformation induces ATP hydrolysis in a bacterial ATP-binding cassette transporter involved in the import of alginate

Received for publication, May 1, 2017, and in revised form, July 12, 2017 Published, Papers in Press, August 2, 2017, DOI 10.1074/jbc.M117.793992

Ai Kaneko[‡1], Kasumi Uenishi[‡1], Yukie Maruyama[§], Nobuhiro Mizuno[¶], Seiki Baba[¶], Takashi Kumasaka[¶], Bunzo Mikami[‖], Kousaku Murata[§], and Wataru Hashimoto[‡2]

From the [‡]Laboratory of Basic and Applied Molecular Biotechnology, Division of Food Science and Biotechnology, and the [‖]Laboratory of Applied Structural Biology, Division of Applied Life Sciences, Graduate School of Agriculture, Kyoto University, Uji, Kyoto 611-0011, Japan, the [§]Laboratory of Food Microbiology, Department of Life Science, Faculty of Science and Engineering, Setsunan University, Neyagawa, Osaka 572-8508, Japan, and the [¶]Japan Synchrotron Radiation Research Institute (JASRI), Sayo-gun, Hyogo 679-5198, Japan

Edited by Wolfgang Peti

The Gram-negative bacterium *Sphingomonas* sp. A1 incorporates alginate into cells via the cell-surface pit without prior depolymerization by extracellular enzymes. Alginate import across cytoplasmic membranes thereby depends on the ATP-binding cassette transporter AlgM1M2SS (a heterotetramer of AlgM1, AlgM2, and AlgS), which cooperates with the periplasmic solute-binding protein AlgQ1 or AlgQ2; however, several details of AlgM1M2SS-mediated alginate import are not well-understood. Herein, we analyzed ATPase and transport activities of AlgM1M2SS after reconstitution into liposomes with AlgQ2 and alginate oligosaccharide substrates having different polymerization degrees (PDs). Longer alginate oligosaccharides (PD ≥ 5) stimulated the ATPase activity of AlgM1M2SS but were inert as substrates of AlgM1M2SS-mediated transport, indicating that AlgM1M2SS-mediated ATP hydrolysis can be stimulated independently of substrate transport. Using X-ray crystallography in the presence of AlgQ2 and long alginate oligosaccharides (PD 6–8) and with the humid air and glue-coating method, we determined the crystal structure of AlgM1M2SS in complex with oligosaccharide-bound AlgQ2 at 3.6 Å resolution. The structure of the ATP-binding cassette transporter in complex with non-transport ligand-bound periplasmic solute-binding protein revealed that AlgM1M2SS and AlgQ2 adopt inward-facing and closed conformations, respectively. These *in vitro* assays and structural analyses indicated that interactions between AlgM1M2SS in the inward-facing conformation and periplasmic ligand-bound AlgQ2 in the closed conformation induce ATP hydrolysis by the ATP-binding protein AlgS. We conclude that substrate-bound AlgQ2 in the closed conformation initially interacts with AlgM1M2SS, the AlgM1M2SS–AlgQ2 complex then forms, and this formation is followed by ATP hydrolysis.

ATP-binding cassette (ABC)[3] transporters are present in cytoplasmic membranes of all species, and the translocation of substrates by transporters is coupled with ATP hydrolysis (1). ABC transporters comprise two transmembrane domains and two nucleotide-binding domains. The transmembrane domains form the translocation pathway, and the nucleotide-binding domains hydrolyze ATP to generate energy for transport (2). ABC transporters are classified as exporters and importers (3), and whereas ABC exporters are ubiquitous from bacteria to humans, ABC importers are mainly found in prokaryotes (4) and require accessory solute-binding proteins (5). Several ABC importers, such as $MalFGK_2$ (6), the maltose transporter in *Escherichia coli*, and the *E. coli* vitamin B_{12} transporter BtuCD (7) have been well-characterized. When importing substrate, ABC importers change conformations from the inward-facing to outward-facing states (5). However, the mechanisms that regulate this conformational change and ATP hydrolysis of ABC importers are not fully understood.

Interactions between the ABC transporter $MalFGK_2$ and the periplasmic maltose-binding protein MalE induce ATP hydrolysis (8). Moreover, a mutant MalE was shown to bind sucrose (non-transport ligand) and enhance the ATPase activity of $MalFGK_2$, suggesting that ATP hydrolysis is induced by ligand-bound MalE but not by the translocated substrate (*i.e.* maltose). Recently, two models of solute-binding protein MalE conformations in contact with $MalFGK_2$ were described as closed (6) and open states (9). However, these findings were based on *in vitro* assays, and the structure of the ABC transporter in complex with the solute-binding protein with a non-transport ligand has not been directly characterized.

This work was supported in part by Grants-in-Aid Scientific Research from the Japan Society for the Promotion of Science (to K. M., Y. M., and W. H.) and the Targeted Proteins Research Program (to W. H.) from the Ministry of Education, Culture, Sports, Science, and Technology (MEXT) of Japan. The authors declare that they have no conflicts of interest with the contents of this article.

The atomic coordinates and structure factors (codes 4XIG, 5H71, 4XTC, and 5H6U) have been deposited in the Protein Data Bank (http://wwpdb.org/).

[1] Both authors contributed equally to this work.

[2] To whom correspondence should be addressed. Tel.: 81-774-38-3766; Fax: 81-774-38-3767; E-mail: whasimot@kais.kyoto-u.ac.jp.

[3] The abbreviations used are: ABC, ATP-binding cassette; M, β-D-mannuronic acid; G, α-L-guluronic acid; FACE, fluorophore-assisted carbohydrate electrophoresis; PA, pyridylamino; HAG, humid air and glue-coating; ADA, *N*-(2-acetamido)iminodiacetic acid; CHAPSO, 3-((3-cholamidopropyl)dimethylammonio)-2-hydroxy-1-propane sulfonate; PVA, polyvinyl alcohol; PD, polymerization degree; RMSD, root mean square deviation; strain A1, *Sphingomonas* sp. strain A1.

Alginate is a linear acidic polysaccharide that comprises β-D-mannuronate (M) and its C-5-epimer α-L-guluronate (G). The Gram-negative and alginate-assimilating bacterium *Sphingomonas* sp. strain A1 incorporates polysaccharides into cells through cell-surface pits (10). Genes that are involved in alginate import and degradation form a cluster on the genome of strain A1 and encode the periplasmic alginate-binding proteins AlgQ1 and AlgQ2; the cytoplasmic membrane-bound ABC transporter (AlgM1M2SS); the cytoplasmic endotype alginate lyases A1-I, A1-II, and A1-III; the exotype alginate lyase (A1-IV); and the alginate-dependent transcription factor AlgO (11, 12). Alginate concentrated in the cell-surface pit is incorporated into the periplasm and is delivered to the ABC transporter by alginate-binding proteins. The ABC transporter for alginate import is a heterotetramer comprising transmembrane domains (heterodimer of AlgM1 and AlgM2) and an ATP-binding domain (homodimer of AlgS). After import into the cytoplasm by the ABC transporter, alginate is depolymerized to monosaccharides by endo- and exotype alginate lyases. Moreover, the genetic cluster for import and degradation of alginate is expressed in the presence of the polysaccharide under the control of the transcription factor AlgO (13).

Characteristics of ATPase and transport activities of reconstituted AlgM1M2SS in liposomes and crystal structures of the transporter have mainly been determined using alginate oligosaccharides with polymerization degrees (PDs) of <4 (14–16). In contrast with the *E. coli* maltose ABC transporter, interactions of AlgM1M2SS with AlgQ2 result in the formation of an alginate-binding tunnel that is accessible to solvent. In the present study, *in vitro* assays of the ATPase and transport activities of AlgM1M2SS were performed using long alginate oligosaccharides (PD ≥ 5), and non-transport ligand–bound AlgQ2 in the closed conformation interacted with the ABC transporter in the inward-facing conformation. These X-ray crystallography structure analyses were performed using the humid air and glue-coating method and demonstrated that the solute-binding protein in the closed conformation induces ATP hydrolysis in this bacterial ABC transporter.

Results

Purification of alginate oligosaccharides

M-rich polysaccharides (M-block) were obtained from alginate, and unsaturated M oligosaccharides with C=C bonds in their non-reducing ends were prepared by treatment of M-block with alginate lyase. Saturated M oligosaccharides were then prepared by acid hydrolysis of M-block, and unsaturated M oligosaccharides were further fractionated by anion exchange chromatography into unsaturated M disaccharide (Δ2M), unsaturated M trisaccharide (Δ3M), unsaturated M tetrasaccharide (Δ4M), unsaturated M pentasaccharide (Δ5M), unsaturated M hexasaccharide (Δ6M), and a mixture of unsaturated M hepta- and octasaccharides (Δ7-8M). Saturated M oligosaccharides were also divided into mixtures of saturated M hexa-, hepta-, and octasaccharides (6–8M) and of saturated M hepta-, octa-, ennea-, and decasaccharides (7–10M) using anion exchange chromatography. PDs in each oligosaccharide were determined using fluorophore-assisted carbohydrate electrophoresis (FACE) (17) (Fig. 1*A*), and the alginate oligosaccharides and their pyridylamino (PA)-saccharides fluorescence-labeled with 2-aminopyridine were used for subsequent experiments.

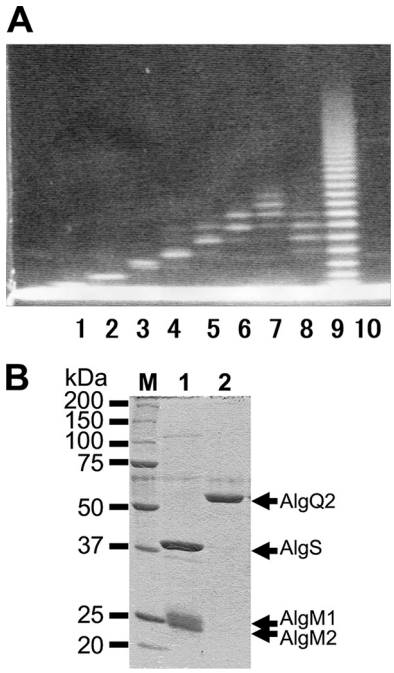

Figure 1. Electrophoretic profiles of oligosaccharides and proteins. *A*, FACE profiles of alginate oligosaccharides. *Lane 1*, Δ2M; *lane 2*, Δ3M; *lane 3*, Δ4M; *lane 4*, Δ5M; *lane 5*, Δ6M; *lane 6*, Δ7-8M; *lane 7*, 7–10M; *lane 8*, 6–8M; *lane 9*, saturated M oligosaccharides before purification; *lane 10*, negative control treated with 8-amino-1,3,6-naphthalenetrisulfonic acid in the absence of oligosaccharide. *B*, SDS-PAGE profiles of AlgM1M2SS (*lane 1*) and AlgQ2 (*lane 2*). Three protein bands indicated by *arrows* correspond to AlgS, AlgM1, and AlgM2 in the purified AlgM1M2SS (*lane 1*). An *arrow* indicates the position of AlgQ2 (*lane 2*). *M*, mass.

Co-immunoprecipitation of AlgQ2 by AlgM1M2SS

Co-immunoprecipitation assays were conducted to analyze interactions between AlgM1M2SS and AlgQ2. In these analyses, recombinant AlgM1M2SS and AlgQ2 were expressed in *E. coli* cells and were purified to homogeneity (Fig. 1*B*). After interactions of anti-His tag antibody conjugated Dynabeads Protein G (Veritas) and AlgM1M2SS containing a histidine tag at the C terminus of AlgM2, AlgQ2 was added in the presence or absence of ATP and Δ3M. Dynabeads Protein G was then collected, and bound proteins were subjected to SDS-PAGE, followed by Western blotting using anti-AlgQ2 antiserum (18) (Fig. 2). AlgQ2 was observed only in the presence of both ATP and Δ3M (Fig. 2, *lanes 2* and *3*), and no interactions between AlgM1M2SS and AlgQ2 occurred in the absence of Δ3M (Fig. 2, *lane 1*). No AlgQ2 was detected in the immunoprecipitation assay using other His tag protein as a negative control in place of AlgM1M2SS (data not shown). Because AlgQ2 comprises N- and C-terminal domains and adopts substrate-free open and substrate-bound closed conformations through domain dynamics (16, 19), these co-immunoprecipitation assays suggested that Δ3M-bound AlgQ2 interacts with AlgM1M2SS in the closed conformation. However, the substrate-free AlgQ2 in the open conformation did not interact with AlgM1M2SS. Moreover, following the addition of vanadate, the intensity of

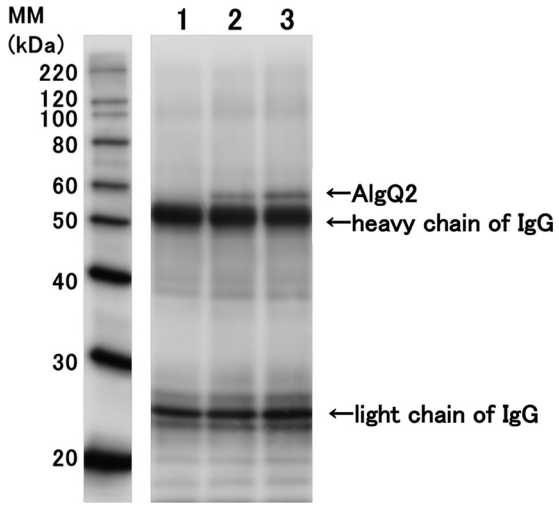

Figure 2. Co-immunoprecipitation of AlgM1M2SS and AlgQ2. *Lane 1*, no ligand; *lane 2*, 2 mM Mg-ATP and 0.2 mM Δ3M; *lane 3*, 2 mM Mg-ATP, 0.2 mM Δ3M, and 5 mM vanadate. *MM*, molecular mass.

the AlgQ2 band increased slightly in the presence of ATP and Δ3M (Fig. 2, *lane 3*). The phosphate analogue vanadate bound the ATP-binding site with ADP and inhibited ATP hydrolysis. Hence, the increase in AlgQ2 band intensity probably reflects inhibited dissociation of AlgQ2 from AlgM1M2SS, suggesting that this dissociation event is coupled with ATP hydrolysis.

ATPase and transport activities of AlgM1M2SS

ATPase and transport activities of reconstituted AlgM1M2SS in liposomes were measured in the presence of various alginate oligosaccharides and AlgQ2 (Fig. 3). Specific ATPase activity of AlgM1M2SS in the absence of saccharide was determined to around 30 nmol/min/mg. In these experiments, all alginate oligosaccharides enhanced ATPase activity, and saccharide chain lengths, structures of non-reducing ends (saturated or unsaturated), and modifications at reducing saccharide residues with PA in alginate oligosaccharides had limited effects on ATPase activities. In contrast, transport activities varied with saccharide chain lengths, with the highest transport activity in the presence of alginate tetrasaccharide as a substrate, and almost no transport of alginate oligosaccharides with PD of >5. In addition, transport of these long oligosaccharides was comparable with that of the non-alginate oligosaccharide chitotetraose, indicating that long alginate oligosaccharides with PD of >5 were not transport substrates of AlgM1M2SS in this assay system.

X-ray diffraction experiments using the humid air and glue-coating (HAG) method

Previously, the crystal structure of AlgM1M2SS was determined in complex with Δ3M-bound AlgQ2 at a resolution of 3.2 Å (14), and similar crystals were frozen using the HAG method (20) to improve X-ray diffraction images. The HAG method is a novel technique for crystal mounting, in which crystals are coated with a water-soluble polymer and are then exposed to controlled humid air using humidifier HUM-1F (RIGAKU). AlgM1M2SS crystals in complex with Δ3M-bound AlgQ2 were obtained in drop solutions comprising 22% PEG 3000, 0.1 M ADA-NaOH (pH 6.6), 0.15 M NaCl, and 16 mM

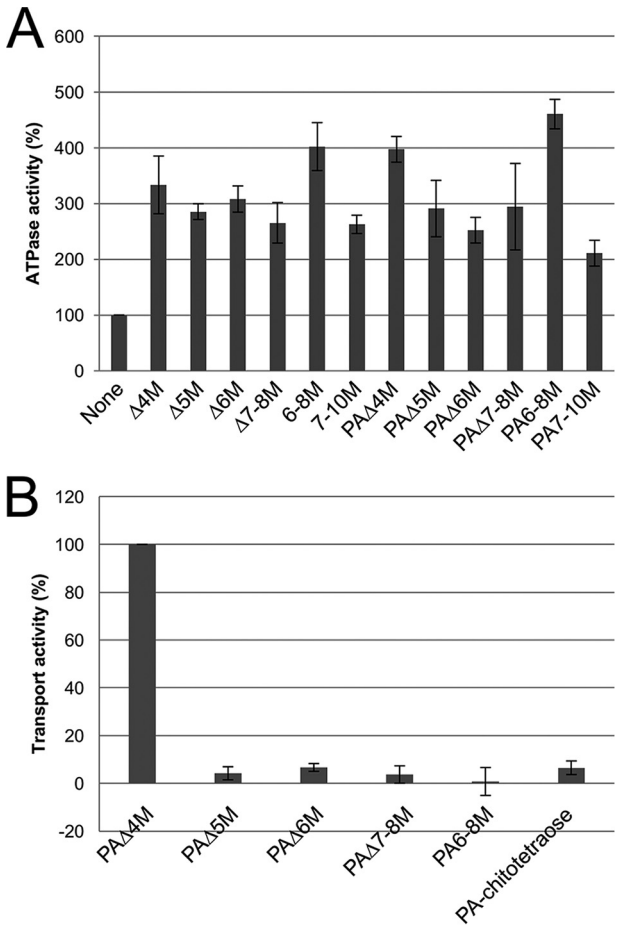

Figure 3. *In vitro* assay of AlgM1M2SS. *A*, ATPase activity; *B*, alginate transport activity; activities are shown as relative values. Activities in the absence of oligosaccharides (*A*) and with Δ4M (*B*) were taken as 100%. Assays were conducted three times, and data are presented as means with *error bars* representing S.E.

CHAPSO. Crystals were then picked up using a loop covered with 10% polyvinyl alcohol (PVA) 4500 and were subjected to X-ray diffraction experiments with air controlled at 86–92% relative humidity. In these experiments, the crystals had optimal mosaicity (0.607) at 90% relative humidity, and after freezing at 90% relative humidity, crystals were exposed to X-rays and provided diffraction data at 3.4 Å resolution, allowing determination of crystal structure by molecular replacement. The overall structure of AlgM1M2SS adopted the inward-facing conformation (Fig. 4*A*), and the electron density map that was obtained using the HAG method included an additional electron density at C-terminal regions of AlgM1 and AlgM2. In contrast with the previous structure, three residues (from Thr-321 to Val-323) in AlgM1 and seven residues (from Gly-285 to Val-291) in AlgM2 were accurately traced in the electron density map, indicating improved X-ray diffraction data after crystal freezing of AlgM1M2SS in complex with AlgQ2 using the HAG method.

To obtain a snapshot of the structure of the ABC transporter in complex with the non-transport ligand-bound solute-binding protein, AlgM1M2SS and AlgQ2 were crystallized in the presence of long alginate oligosaccharides. In these experiments, crystals of AlgM1M2SS, AlgQ2, and 6–8M were

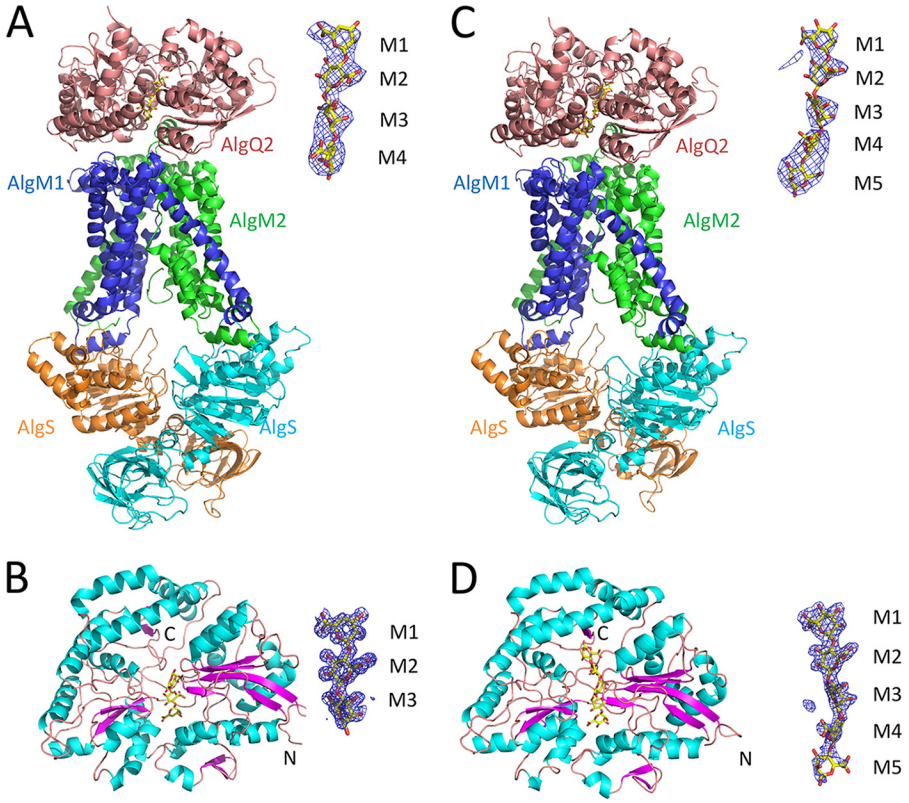

Figure 4. Overall structure. The *images* on the *right* show the $F_o - F_c$ map contoured at 2.8σ around the alginate oligosaccharide. *A*, AlgM1M2SS/AlgQ2 + Δ3M; *B*, AlgQ2 + Δ3M; *C*, AlgM1M2SS/AlgQ2 + 6–8M; *D*, AlgQ2 + 7–10M.

obtained in a drop solution comprising 22% PEG 3000, 0.1 M ADA-NaOH (pH 6.6), 0.15 M sodium formate, 8 mM CHAPSO, and 4 mM ATP and were picked up using a loop covered with 10% PVA 4500 and 5% ethylene glycol for X-ray diffraction experiments with controlled humid air. Dehydration of the crystal at 85% relative humidity for 10 min significantly improved mosaicity (1.714–0.732), which was reduced to 0.846 at 83% relative humidity. The crystal was finally frozen and subjected to X-ray diffraction experiments at 85% relative humidity. Subsequently, the crystal structure of AlgM1M2SS in complex with long alginate oligosaccharide-bound AlgQ2 was determined at 3.6 Å using molecular replacement. In the resulting complex, AlgM1M2SS and AlgQ2 adopted the inward-facing and closed conformations, respectively (Fig. 4*C*). However, although crystallization was conducted in the presence of ATP, no density map of ATP was observed. Diffraction data and refinement statistics are shown in Table 1.

Alginate recognition by AlgQ2 in the complex

In addition to AlgM1M2SS in complex with long alginate oligosaccharide-bound AlgQ2, crystal structures of AlgQ2 complexed with Δ3M and 7–10M were determined to analyze configurations of oligosaccharides bound to AlgQ2. The crystal of Δ3M-bound AlgQ2 was then generated in drop solution comprising 30% PEG 4000, 0.1 M Tris-HCl (pH 8.5), and 0.2 M $LiSO_4$. AlgQ2 was also co-crystallized with 7–10M in drop solution comprising 25% PEG 4000, 0.1 M Tris-HCl (pH 8.5), and 0.2 M calcium chloride. Finally, crystal structures of Δ3M- and 7–10M-bound AlgQ2 were determined by molecular replacement at 1.55 and 2.0 Å resolution, respectively, and overall structures of both were shown to adopt the closed conformation (Fig. 4, *B* and *D*).

The present structures of AlgM1M2SS in complex with Δ3M and 6–8M-bound AlgQ2 were essentially the same as the previously determined structure (Protein Data Bank entry 4TQU), with root mean square deviations (RMSDs) of <0.6 Å for 1641 Cα atoms. Moreover, no significant differences between structures of AlgM1M2SS in complex with Δ3M and 6–8M-bound AlgQ2 were observed at the AlgM1M2SS–AlgQ2 interface, suggesting that saccharide chain lengths had no effects on structures and conformations of AlgM1M2SS and AlgQ2.

The electron density map corresponded to four saccharide residues of AlgQ2 in the complex of AlgM1M2SS and Δ3M-bound AlgQ2, whereas three saccharide residues in Δ3M were bound to AlgQ2 in a monomer form (Fig. 4, *A* and *B*). These observations suggest two binding modes of Δ3M in the AlgQ2 interaction with AlgM1M2SS. However, the present data were insufficient for analyses of occupancy and conformations of the two trisaccharides in the complex of AlgM1M2SS and Δ3M-bound AlgQ2, and the coordinates corresponding to a tetrasaccharide were included for convenience. AlgQ2 recognizes the first to fourth saccharide residues from the non-reducing end of the substrate at subsites 1–4 (15, 16, 19). In the structure of AlgM1M2SS complexed with Δ3M-bound AlgQ2, Δ3M was accommodated at subsites 1–3 or subsites 2–4 in AlgQ2, and in the latter scenario, Δ3M was considered a translocation product of Δ3M at subsites 1–3 with the slide of one residue.

Table 1
Crystallization conditions, data collection, and structure refinement

	AlgM1M2SS/AlgQ2 + 6–8M	AlgQ2 + 7–10M	AlgM1M2SS/AlgQ2 + Δ3M	AlgQ2 + Δ3M
Crystallization conditions				
Sample solution	7 mg/ml AlgM1(d24) M2(H10)SS(E160Q) 3.5 mg/ml AlgQ2 2 mM 6–8M 8 mM CHAPSO	 3 mg/ml AlgQ2 1 mM 7–10M	7 mg/ml AlgM1(d24) M2(H10)SS(E160Q) 3.5 mg/ml AlgQ2 2 mM Δ3M 16 mM CHAPSO	 3 mg/ml AlgQ2 1 mM Δ3M
Reservoir solution	22% PEG 3000 0.1 M ADA-NaOH (pH 6.6) 0.15 M HCOONa	25% PEG 4000 0.1 M Tris-HCl (pH 8.5) 0.2 M $CaCl_2$	22% PEG 3000 0.1 M ADA-NaOH (pH 6.6) 0.15 M NaCl	30% PEG 4000 0.1 M Tris-HCl (pH 8.5) 0.2 M Li_2SO_4
Data collection				
Beam line	SPring-8 BL38B1	SPring-8 BL26B2	SPring-8 BL38B1	SPring-8 BL38B1
Detector	MX225HE (Rayonix)	MX225 (Rayonix)	Quantum315r (Area Detector Systems Corp.)	MX225HE (Rayonix)
Detector–crystal distance (mm)	250	175	350	130
HAG conditions				
Glue	10% PVA 4500, 5% ethylene glycol		10% PVA 4500	
Optimized humidity (%)	85		90	
Wavelength (Å)	1.0000	1.0000	1.0000	1.0000
Resolution range (Å)	50.0–3.60 (3.66–3.60)[a]	50.0–2.00 (2.03–2.00)	50.0–3.40 (3.46–3.40)	30–1.55 (1.58–1.55)
Space group	$P2_12_12_1$	$P1$	$P2_12_12_1$	$P2_1$
Unit-cell parameters				
a, b, c (Å)	71.6, 133.0, 273.0	46.1, 59.2, 82.7	72.2, 133.4, 272.7	76.3, 53.2, 127.5
α, β, γ (degrees)		84.7, 90.2, 88.0		90, 93.6, 90
No. of molecules/asymmetric unit	1	2	1	2
Total observations	144,544	173,757	266,184	539,873
Unique reflections	30,118	56,452	37,120	143,400
Completeness (%)	95.6 (98.0)	97.4 (96.1)	99.8 (100)	96.8 (94.4)
$I/\sigma(I)$	21.4 (3.2)	31.4 (5.6)	36.9 (4.1)	25.9 (3.2)
R_{merge}	0.042 (0.461)	0.053 (0.157)	0.046 (0.536)	0.084 (0.420)
$CC_{1/2}$ in outer shell (%)	80.2	95.2	85.3	85.8
Mosaicity (degrees)	1.014	1.510	0.634	0.524
Refinement				
Resolution range (Å)	37.4–3.60 (3.72–3.60)	35.7–2.01 (2.04–2.01)	37.6–3.40 (3.49–3.40)	29.9–1.55 (1.57–1.55)
R_{work}/R_{free}	0.238/0.289 (0.286/0.338)	0.201/0.261 (0.264/0.325)	0.236/0.290 (0.271/0.327)	0.167/0.196 (0.214/0.228)
No. of atoms				
Protein	14,207	8012	14,222	8130
Alginate	61	122	48	72
Water	0	564	0	481
Calcium ion	0	6	0	2
Chloride ion	0	0	0	2
PEG	0	0	0	64
RMSD				
Bond lengths (Å)	0.003	0.010	0.003	0.007
Bond angles (degrees)	0.781	1.041	0.820	1.126
Ramachandran plot				
Most favored (%)	93.32	97.94	92.26	97.97
Allowed (%)	6.23	1.96	7.34	2.03
Outlier (%)	0.45	0.10	0.39	0

[a] Data in the highest-resolution shell are shown in parentheses.

This translocation of Δ3M was probably carried out through docking of Δ3M-bound AlgQ2 and the ABC transporter AlgM1M2SS.

In structures of the AlgM1M2SS and AlgQ2 complex and AlgQ2 alone, the electron density map corresponded to only five saccharide residues of AlgQ2, despite the addition of 6–8M to the crystallization drop solution (Fig. 4, *C* and *D*). Hence, AlgQ2 may strictly recognize five saccharide residues of alginate, and the sixth or later saccharide residue is flexible due to limited interactions with AlgQ2.

Structures of the substrate-binding site of AlgQ2 in four kinds of crystals are presented in Fig. 5. Tables 2 and 3 show amino acid residues of AlgQ2 interacting with saccharide residues via hydrogen bonds (<3.5 Å) and C–C interactions (<4.4 Å), respectively. The interaction of AlgQ2 with AlgM1M2SS produced little effect on the structure of the subsite in AlgQ2 (Fig. 5) or on the substrate-binding mode (Tables 2 and 3). Saccharide residues are represented as M1, M2, M3, M4, and M5 in that order from the non-reducing end. As reported previously (16), the number of hydrogen bonds between residues of amino acids and saccharides was greatest in M1, confirming that AlgQ2 strongly recognizes the saccharide of the non-reducing end. M5 also formed C–C interactions with multiple amino acid residues, suggesting that AlgQ2 recognizes alginate at subsites 1–5.

Discussion

ABC importers are classified as type I or II based on their structures. Type I ABC transporters include the maltose transporter $MalFGK_2$ and AlgM1M2SS, whereas the vitamin B_{12} transporter BtuCD is categorized as a type II ABC transporter. $MalFGK_2$ exhibits significant ATPase activity in the presence of both maltose-binding protein (MalE) and maltose, whereas the MalE mutant (sMBP) accommodates maltose and sucrose, which is a non-transport substrate. $MalFGK_2$ reportedly exhibited similar ATPase activity in the presence of sMBP and either maltose or sucrose (8), suggesting that ATP hydrolysis is induced by interactions between the ABC transporter and the solute-binding protein with any substrate, but not by translo-

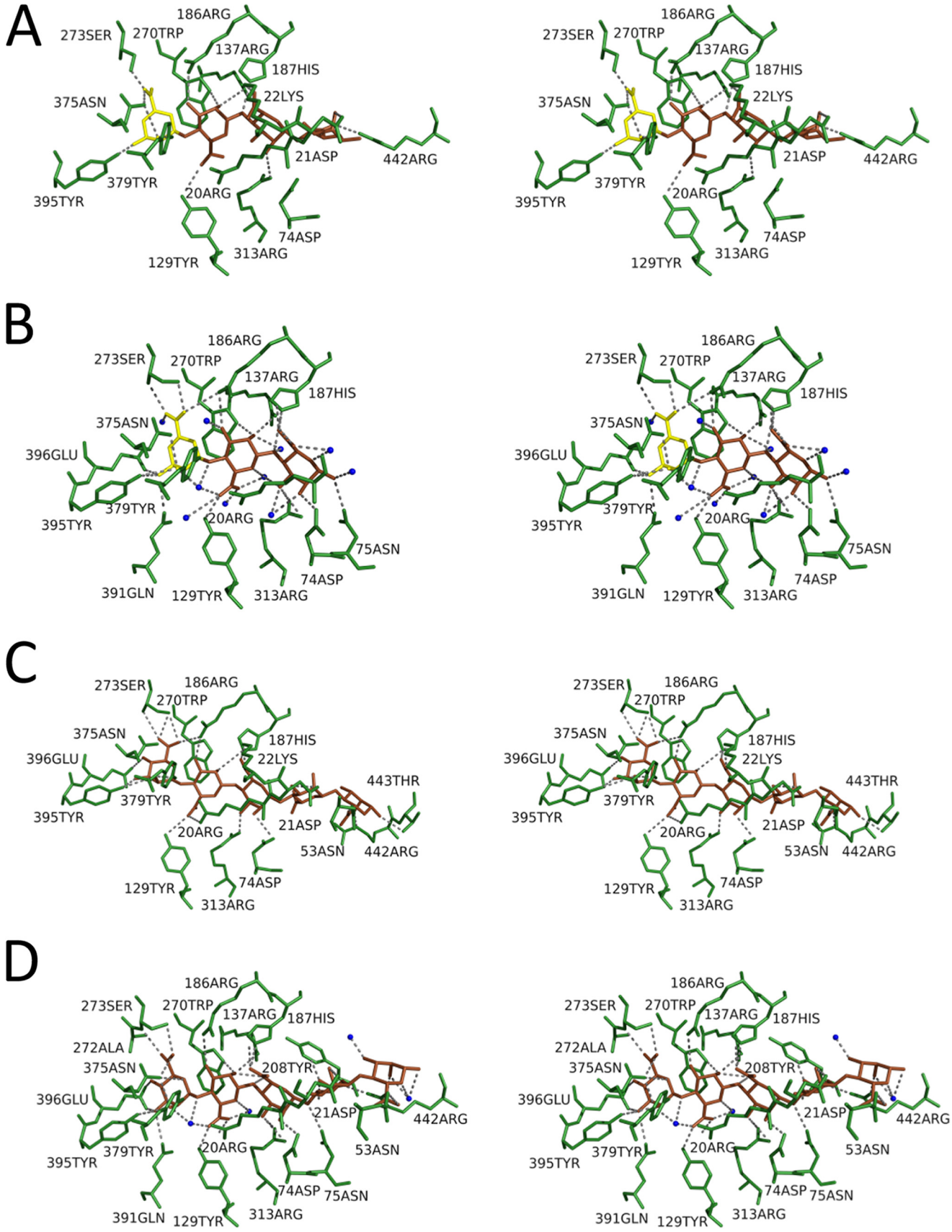

Figure 5. *Cross-eyed stereo views* of the alginate-binding site of AlgQ2. *A*, AlgM1M2SS/AlgQ2 + Δ3M; *B*, AlgQ2 + Δ3M; *C*, AlgM1M2SS/AlgQ2 + 6–8M; *D*, AlgQ2 + 7–10M. ΔM and M are shown as *yellow* and *brown saccharides*, respectively. Water molecules are shown as *blue spheres*. *Dotted lines*, hydrogen bonds.

Table 2
Hydrogen bond between AlgQ2 and alginate oligosaccharide

AlgM1M2SS/AlgQ2 + 6–8M					AlgQ2 + 7–10M					AlgM1M2SS/AlgQ2 + Δ3M					AlgQ2 + Δ3M				
Sugar	Atom	Amino acid	Atom	Distance	Sugar	Atom	Amino acid	Atom	Distance	Sugar	Atom	Amino acid	Atom	Distance	Sugar	Atom	Amino acid	Atom	Distance
				Å					Å					Å					Å
M1	O2	Tyr-379	OH	3.0	M1	O2	Asn-375	ND2	3.3	M1	O2	Asn-375	ND2	3.3	M1	O2	Asn-375	ND2	3.1
M1	O2	Tyr-395	OH	3.4	M1	O2	Tyr-395	OH	3.1	M1	O2	Tyr-379	OH	2.9	M1	O2	Tyr-395	OH	3.1
M1	O3	Tyr-395	OH	2.2	M1	O3	Gln-391	NE2	3.2	M1	O3	Tyr-395	OH	2.3	M1	O3	Gln-391	NE2	3.3
M1	O4	Glu-396	OE2	3.5	M1	O3	Tyr-395	OH	2.5	M1	O6A	Ser-273	OG	2.2	M1	O3	Tyr-395	OH	2.6
M1	O6A	Ser-273	OG	3.0	M1	O3	Glu-396	OE1	3.0	M1	O6A	Asn-375	ND2	2.7	M1	O3	Glu-396	OE1	2.7
M1	O6A	Ser-273	N	3.4	M1	O4	Glu-396	OE1	3.5						M1	O5	Asn-375	ND2	3.2
M1	O6B	Ser-273	OG	3.2	M1	O4	Glu-396	OE2	3.1						M1	O6A	Arg-186	NH2	3.5
					M1	O5	Asn-375	ND2	3.4						M1	O6A	Ser-273	OG	2.6
					M1	O6A	Ser-273	OG	2.9						M1	O6A	Asn-375	ND2	3.0
					M1	O6A	Asn-375	ND2	3.2						M1	O6B	Ser-273	N	2.9
					M1	O6B	Ser-273	N	3.0						M1	O6B	Ser-273	OG	3.4
M2	O2	His-187	NE2	3.5	M2	O2	Arg-137	NH2	3.2	M2	O2	Trp-270	NE1	3.0	M2	O2	Trp-270	NE1	3.0
M2	O2	Trp-270	NE1	3.3	M2	O2	Trp-270	NE1	2.6	M2	O2	Arg-137	NH2	3.5	M2	O2	Arg-137	NH2	3.1
M2	O3	Arg-186	NH2	2.6	M2	O3	Arg-186	NH2	3.0	M2	O3	Arg-186	NH2	2.7	M2	O2	His-187	NE2	3.4
M2	O4	Tyr-379	OH	2.9	M2	O3	Trp-270	NE1	3.1	M2	O6A	Tyr-129	OH	3.3	M2	O3	Arg-186	NH2	3.0
M2	O6B	Arg-20	NH2	3.5	M2	O4	Tyr-379	OH	3.5						M2	O3	Trp-270	NE1	3.3
M2	O6B	Tyr-129	OH	3.1	M2	O6B	Tyr-129	OH	2.6						M2	O4	Tyr-379	OH	3.5
															M2	O6A	Tyr-129	OH	2.6
M3	O2	Asp-74	OD2	3.3						M3	O2	Arg-313	NH2	3.3	M3	O1	Asp-74	OD2	3.5
M3	O3	Arg-313	NH2	2.3	M3	O2	Asp-74	OD2	2.9	M3	O4	His-187	NE2	2.8	M3	O1	Asn-75	ND2	2.7
M3	O6A	His-187	NE2	2.8	M3	O3	Arg-313	NH1	3.3	M3	O6A	Lys-22	NZ	2.5	M3	O2	Asp-74	OD2	2.8
M3	O6B	Lys-22	NZ	3.0	M3	O3	Arg-313	NH2	3.3	M3	O6B	Lys-22	NZ	3.3	M3	O3	Arg-313	NH1	3.2
					M3	O6A	His-187	NE2	3.3						M3	O3	Arg-313	NH2	3.2
															M3	O4	His-187	NE2	3.4
															M3	O6A	His-187	NE2	2.7
M4	O3	Asp-21	OD2	3.4	M4	O2	Asp-21	OD2	3.2	M4	O2	Asp-21	OD2	3.4					
					M4	O4	Asp-74	OD2	3.4	M4	O3	Arg-20	O	3.5					
					M4	O4	Asn-75	ND2	2.9	M4	O4	Asp-74	OD2	3.4					
					M4	O6A	Arg-442	NH2	3.2	M4	O6B	Arg-442	NH2	3.0					
M5	O1	Thr-443	OG1	2.8	M5	O2	Arg-442	NH1	2.4										
M5	O2	Arg-442	NE	2.5	M5	O6A	Asn-53	ND2	3.5										
M5	O2	Arg-442	NH2	3.4															
M5	O6B	Asn-53	ND2	2.5															

cation of the substrate by the ABC transporter. However, the structure of the $MalFGK_2$ and sucrose-bound sMBP complex has not been determined, and the initial interaction mode between the ABC transporter and solute-binding protein remains unknown. In contrast, when present in excess of ATP (ATP/ABC transporter = 1:20), the ATPase activity of $MalFGK_2$ in the presence of MalE was higher than that in the presence of both MalE and maltose (9). These observations suggest that interactions between MalE in the open conformation and $MalFGK_2$ induce ATP hydrolysis. Accordingly, in the presence of excess ATP (ATP/ABC transporter = 1000:1), ATPase activity of $MalFGK_2$ in the presence of MalE and maltose was higher than that in the presence of MalE alone, suggesting that MalE interacts with $MalFGK_2$ in closed and open conformations (6). Because the complex structure of $MalFGK_2$ and MalE has not yet been characterized at the moment of formation, the ensuing interaction scheme remains controversial. Similarly, the solute-binding protein BtuF reportedly induces ATP hydrolysis activity of the type II transporter BtuCD (21), although the details of the interaction scheme between BtuCD and BtuF are not fully understood.

The present *in vitro* assays indicated that long alginate oligosaccharides with PD of >5 were not transported by liposome-reconstituted AlgM1M2SS. Moreover, in alginate-importing A1 cells, AlgM1M2SS is expressed in conjunction with cell-surface pits (11), suggesting that the ABC transporter requires additional elements, such as the cell-surface pit, for import of alginate polymers. However, long alginate oligosaccharides with PD of >5 stimulated ATPase activity of AlgM1M2SS, suggesting that substrate binding by the solute-binding protein triggers ATP hydrolysis in AlgM1M2SS. Accordingly, X-ray crystallography demonstrated that long alginate oligosaccharide-bound AlgQ2 in the closed conformation interacts with AlgM1M2SS. To the best of our knowledge, this is the first structural characterization of the complex of the ABC transporter with the non-transport ligand-bound solute-binding protein.

Although the structure of the AlgM1M2SS and Δ3M-bound AlgQ2 complex was determined previously, it remains unclear which step of the transport cycle was structurally characterized, because Δ3M was used as a transport substrate of AlgM1M2SS. In contrast, the complex structure of AlgM1M2SS with non-transport 6–8M-bound AlgQ2 is indicative of the initial moment of the interaction between AlgQ2 and AlgM1M2SS. This structure indicates that ATP binding and hydrolysis occur after the formation of the complex, because no ATP is included in the complex structure (Fig. 6). In conclusion, substrate-bound AlgQ2 in the closed conformation initially interacts with AlgM1M2SS, and the AlgM1M2SS–AlgQ2 complex forms subsequently, followed by ATP hydrolysis.

Experimental procedures

Preparation and fluorescence labeling of alginate oligosaccharides

M oligosaccharides were prepared from alginate as reported previously (15). Briefly, alginate was hydrolyzed using HCl and was divided into M-block– and G–rich saccharides (G-block)

Table 3
C–C interaction between AlgQ2 and alginate oligosaccharide

AlgM1M2SS/AlgQ2 + 6–8M					AlgQ2 + 7–10M					AlgM1M2SS/AlgQ2 + Δ3M					AlgQ2 + Δ3M				
Sugar	Atom	Amino acid	Atom	Distance	Sugar	Atom	Amino acid	Atom	Distance	Sugar	Atom	Amino acid	Atom	Distance	Sugar	Atom	Amino acid	Atom	Distance
				Å					Å					Å					Å
M1	C4	Trp-399	CH2	4.4	M1	C1	Trp-270	CD2	4.0	M1	C1	Trp-270	CE2	4.4	M1	C1	Trp-270	CZ3	3.9
M1	C4	Trp-399	CZ2	4.3	M1	C1	Trp-270	CE3	4.1	M1	C1	Trp-270	CD2	4.3	M1	C1	Trp-270	CH2	4.0
M1	C5	Trp-270	CB	4.3	M1	C1	Trp-270	CE2	4.0	M1	C1	Trp-270	CE3	4.0	M1	C1	Trp-270	CD2	3.9
M1	C5	Trp-270	CG	4.2	M1	C1	Trp-270	CZ2	4.1	M1	C1	Trp-270	CZ3	3.7	M1	C1	Trp-270	CE3	3.9
M1	C5	Trp-270	CD2	4.0	M1	C1	Trp-270	CZ3	4.1	M1	C1	Trp-270	CH2	3.8	M1	C1	Trp-270	CE2	4.0
M1	C5	Trp-270	CE3	3.9	M1	C1	Trp-270	CH2	4.2	M1	C1	Trp-270	CZ2	4.2	M1	C1	Trp-270	CZ2	4.1
M1	C6	Ser-273	CB	4.0	M1	C3	Glu-396	CD	3.9	M1	C3	Glu-396	CD	4.2	M1	C3	Glu-396	CD	4.0
M1	C6	Trp-270	CD1	4.2	M1	C4	Trp-399	CH2	4.1	M1	C4	Glu-396	CD	4.3	M1	C3	Trp-270	CZ3	4.1
M1	C6	Trp-270	CB	3.3	M1	C4	Trp-399	CZ2	4.2	M1	C4	Trp-399	CH2	4.0	M1	C3	Trp-270	CE3	4.2
M1	C6	Trp-270	CG	3.5	M1	C4	Glu-396	CD	4.0	M1	C4	Trp-399	CZ2	4.2	M1	C4	Glu-396	CD	3.7
M1	C6	Trp-270	CD2	3.8	M1	C5	Trp-270	CB	3.8	M1	C5	Trp-270	CD2	4.3	M1	C4	Trp-270	CZ3	4.3
M1	C6	Trp-270	CE3	4.1	M1	C5	Trp-270	CG	3.8	M1	C5	Trp-270	CE3	4.0	M1	C4	Trp-270	CE3	3.8
					M1	C5	Trp-270	CD2	3.6	M1	C6	Trp-399	CH2	4.1	M1	C5	Asn-375	CG	4.4
					M1	C5	Trp-270	CE3	3.6	M1	C6	Trp-270	CG	4.3	M1	C5	Trp-270	CZ3	4.4
					M1	C5	Trp-270	CZ3	4.4	M1	C6	Trp-270	CD2	4.4	M1	C5	Trp-270	CB	4.0
					M1	C6	Ser-273	CB	3.6	M1	C6	Trp-270	CE3	4.3	M1	C5	Trp-270	CG	4.0
					M1	C6	Ser-273	CA	4.4	M1	C6	Trp-270	CB	4.0	M1	C5	Trp-270	CD2	3.8
					M1	C6	Trp-399	CH2	4.1	M1	C6	Ser-273	CB	4.0	M1	C5	Trp-270	CE3	3.7
					M1	C6	Trp-270	CB	3.4						M1	C6	Ser-273	CB	3.7
					M1	C6	Trp-270	CG	3.8						M1	C6	Asn-375	CG	4.3
					M1	C6	Trp-270	CD2	4.2						M1	C6	Trp-399	CH2	4.1
															M1	C6	Trp-270	CB	3.3
															M1	C6	Trp-270	CG	3.8
															M1	C6	Trp-270	CD2	4.1
															M1	C6	Trp-270	CE3	4.2
M2	C2	His-187	CE1	4.3	M2	C2	His-187	CE1	3.9	M2	C2	Arg-186	CZ	4.4	M2	C2	His-187	CE1	3.7
M2	C5	Arg-20	CZ	4.2	M2	C2	Trp-270	CE2	4.4	M2	C2	His-187	CE1	3.9	M2	C3	Trp-270	CE2	4.3
M2	C6	Tyr-129	CE2	4.3	M2	C3	Trp-270	CD1	4.3	M2	C4	Trp-270	CE2	4.3	M2	C4	Trp-270	CH2	4.4
					M2	C3	Trp-270	CE2	4.2	M2	C4	Trp-270	CH2	4.3	M2	C4	Trp-270	CE2	3.9
					M2	C4	Trp-270	CE2	3.9	M2	C4	Trp-270	CZ2	4.0	M2	C4	Trp-270	CZ2	3.8
					M2	C4	Trp-270	CZ2	3.8						M2	C6	Tyr-129	CZ	4.3
					M2	C5	Arg-20	CZ	4.3						M2	C6	Tyr-129	CE2	4.1
					M2	C6	Tyr-129	CZ	4.3						M2	C6	Arg-313	CD	4.3
					M2	C6	Tyr-129	CE2	4.1										
					M3	C2	Arg-313	CZ	4.2	M3	C4	His-187	CD2	4.4	M3	C2	Arg-313	CZ	4.1
					M3	C3	Arg-313	CZ	4.1	M3	C5	His-187	CD2	3.9	M3	C3	Arg-313	CZ	4.0
					M3	C4	Arg-20	CG	4.3	M3	C6	Arg-20	CD	4.4	M3	C5	His-187	CD2	4.0
					M3	C4	Arg-20	CD	4.4	M3	C6	Lys-22	CE	4.2	M3	C6	His-187	CD2	4.0
					M3	C5	His-187	CD2	4.3										
					M3	C5	Arg-20	CG	4.4										
					M3	C6	Arg-20	CB	4.2										
					M3	C6	His-187	CD2	4.3										
					M3	C6	Arg-20	CG	4.0										
					M3	C6	Arg-20	CD	4.2										
M4	C2	Asp-21	CG	4.3	M4	C2	Asp-21	CG	3.7	M4	C2	Asp-21	CG	4.0					
M4	C3	Asp-21	CG	4.2	M4	C3	Asp-21	CG	4.3	M4	C3	Arg-20	CA	3.9					
					M4	C6	Tyr-208	CD2	4.3	M4	C3	Arg-20	C	4.4					
										M4	C5	Asn-75	CG	4.3					
M5	C1	Arg-442	CD	4.2	M5	C1	Tyr-446	CG	4.4										
M5	C1	Thr-443	CA	4.4	M5	C2	Tyr-446	CE1	4.3										
M5	C2	Arg-442	CD	4.1	M5	C2	Tyr-446	CG	3.8										
M5	C2	Tyr-446	CG	4.2	M5	C2	Tyr-446	CD1	4.2										
M5	C2	Tyr-446	CD2	4.4	M5	C2	Tyr-446	CZ	4.1										
M5	C2	Tyr-446	CB	4.2	M5	C2	Tyr-446	CE2	3.7										
M5	C3	Tyr-446	CG	4.4	M5	C2	Tyr-446	CD2	3.6										
M5	C3	Tyr-446	CD2	4.3	M5	C3	Tyr-446	CZ	4.3										
					M5	C3	Tyr-446	CE2	4.1										
					M5	C6	Gln-55	CG	4.3										

based on differences in the solubility at pH 2.85. Treatment of neutralized M-block with alginate lyase provided unsaturated M oligosaccharides, and acid hydrolysis of M-block with HCl provided saturated M oligosaccharides. M oligosaccharides were then labeled with 2-aminopyridine as reported previously (14) and were then eluted through a HiTrap Q HP column (GE healthcare). Remaining reagents and unreacted oligosaccharides were excluded using anion exchange chromatography, and purified PA-saccharides were obtained.

FACE

FACE (17) was conducted to determine the purity of alginate oligosaccharides, which were then mixed with labeling reagent containing 75 mM 8-amino-1,3,6-naphthalenetrisulfonic acid, 0.5 M sodium cyanoborohydride, 7.5% (v/v) acetic acid, and 50% (v/v) dimethyl sulfoxide and were incubated at 37 °C for 16 h in the shade. Labeled alginate oligosaccharides were then freeze-dried and resolved in 10% glycerol and were then subjected to electrophoresis in 30% polyacrylamide gels with running buffer containing 25 mM Tris-HCl (pH 8.5) and 0.192 M glycine. Bands of labeled oligosaccharides in gels were detected using an ultraviolet lamp.

Assays of ATPase and transport activities

Expression and purification of AlgM1M2SS was conducted as reported previously (14). Briefly, *E. coli* BL21(DE3)Gold

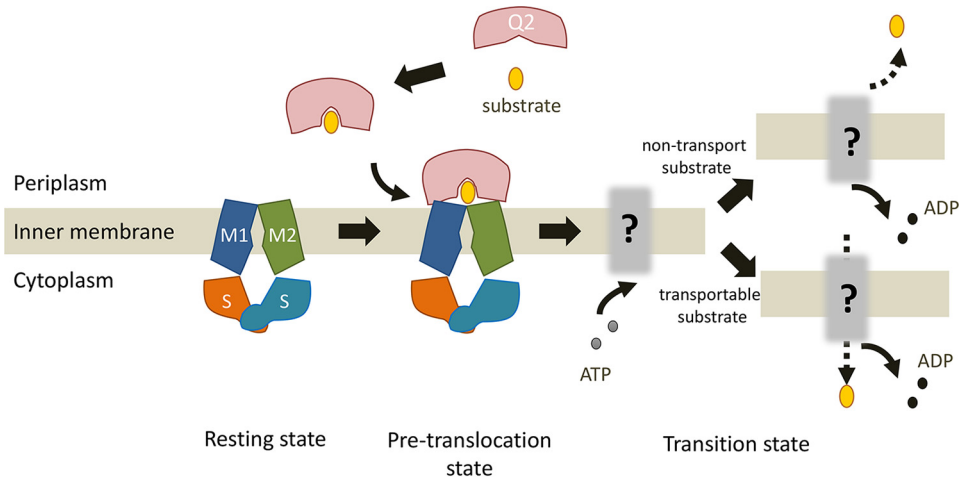

Figure 6. A model for ATP hydrolysis by periplasmic solute-binding protein–dependent ABC transporter. The model shows the following steps: (i) resting state before docking of AlgM1M2SS and AlgQ2; (ii) pretranslocation state at the moment of interaction between AlgM1M2SS in the inward-facing conformation and ligand-bound AlgQ2 in the closed conformation; (iii) docking-dependent ATP binding and hydrolysis; and (iv) substrate import or return to resting state in the case of non-transport substrate.

cells were transfected with the expression plasmid pET21b_AlgM1(d0)M2(H10)SS(WT), in which a histidine tag is attached to the C terminus of AlgM2, and AlgM1 and AlgS are encoded by wild-type sequences. The same strain was used as a host for the expression plasmid pET21b_AlgM1(d24)M2(H10)SS(E160Q), in which the encoded AlgS lacks ATPase activity and 2–24 residues of the N terminus of AlgM1 have been truncated. Membrane fractions were prepared by ultracentrifugation from cell extracts of *E. coli*. After solubilization with the surfactant *n*-dodecyl-β-D-maltoside, AlgM1M2SS was purified using a nickel-nitrilotriacetic acid column (Qiagen) and a Hi Load 16/60 Superdex 200 PG column (GE Healthcare), and expression and purification of AlgQ2 were conducted as reported previously (19). *E. coli* cell extracts were eluted through a HiTrap SP HP column (GE Healthcare) and a Hi Load 16/60 Superdex 200 PG column.

Proteoliposomes were prepared using L-α-phosphatidylcholine (Sigma-Aldrich) and phospholipid derived from soybean as reported previously (14). ATPase assays were performed using type II-S, whereas transport assays were performed using type IV-S. AlgM1M2SS was added to liposomes that were destabilized in *n*-octyl-β-D-glucoside and were diluted to less than critical micelle concentrations to produce proteoliposomes. Magnesium ions and ATP were confined in proteoliposomes for transport assays (14).

Assays of ATPase and transport activity were conducted as reported previously (14). Briefly, reactions were conducted in the presence of 0.1 μM AlgM1M2SS, 1 μM AlgQ2, 5 mM Mg-ATP, and 20 μM oligosaccharides. ATPase activity was determined as the amount of inorganic phosphate released per min, and transport activity was measured in the presence of PA-saccharides. The reaction mixture comprised 0.1 μM AlgM1M2SS, 1.3 μM AlgQ2, 2 mM ATP, 10 mM $MgCl_2$, 20 μM PA-saccharide, and 20 mM Tris-HCl (pH 8.0). Liposomes were collected by ultracentrifugation after reactions, and transport activities were determined based on fluorescence intensities of imported PA-saccharides.

Co-immunoprecipitation assays

Interactions between AlgM1M2SS and AlgQ2 were determined using co-immunoprecipitation assays with binding/washing buffer comprising 10% glycerol, 0.1 M NaCl, 0.045% 6-cyclohexyl-hexyl-β-D-maltoside, 0.25% CHAPSO, and 20 mM Tris-HCl (pH 8.0). AlgM1M2SS exhibits significant ATPase activity in this surfactant solution. Precipitates were collected from 30 μl of Dynabeads Protein G using DynaMag-2 (Life Technologies) and were then mixed with 200 μl of binding buffer containing 0.5 μg of rabbit anti-His-tag antibody (Cosmo Bio). After incubation at 4 °C for 15 min, precipitates were washed once with wash buffer, and 200 μl of binding buffer containing 20 μg of AlgM1(d24)M2(H10)SS(WT) was added. After incubation at 4 °C for 15 min, precipitates were washed once with wash buffer, and 200-μl aliquots of binding buffers containing 20 μg of AlgQ2, 0 or 2 mM Mg-ATP, 0 or 0.2 mM Δ3M, and 0 or 5 mM sodium orthovanadate were added. After incubation at 4 °C for 15 min, precipitates were washed four times in wash buffer and were then dissolved in 10-μl aliquots of binding buffer and 10 μl of 2× SDS buffer comprising 4% SDS, 12% 2-mercaptoethanol, 20% glycerol, 0.1 M Tris-HCl (pH 6.8), and bromphenol blue. After boiling for 3 min, mixtures were centrifuged, and supernatants were subjected to SDS-PAGE analyses. AlgQ2 was then detected in Western blots using rabbit anti-AlgQ2 antiserum as a primary antibody and donkey anti-rabbit IgG as a secondary antibody (GE Healthcare).

Crystallization and X-ray diffraction experiments

Crystallization and crystal freezing of AlgQ2 (15) and crystallization of the AlgM1(d24)M2(H10)SS(E160Q) and AlgQ2 complex (14) were conducted as reported previously. Crystals of AlgM1(d24)M2(H10)SS(E160Q) and AlgQ2 complexes were frozen using the HAG method (20). Crystals were picked up using a loop covered with 10% PVA 4500 with or without ethylene glycol and were frozen in a cold nitrogen gas stream at optimized humidity.

Analysis of diffraction data

Diffraction data from frozen crystals were collected at a wavelength of 1.0000 Å using a BL38B1 or BL26B2 beamline in SPring-8 (Hyogo, Japan) and were processed using HKL2000 (22). Phases were solved by molecular replacement using Molrep (23) in CCP4 interface (24) with the structure of the AlgM1M2SS and AlgQ2 complex (Protein Data Bank entry 4TQU or 4XIG) or the structure of AlgQ2 as initial search models. Structures were refined using Refmac5 (25) and phenix.refine (26), and model construction was performed using WinCoot (27). The figures of structures were produced using PyMOL (28). Interactions between oligosaccharides and proteins were investigated using the program Contact in the CCP4 interface. RMSD values were calculated using PyMOL.

Author contributions—A. K., K. U., and S. B. performed the experiments. A. K., K. U., Y. M., N. M., S. B., T. K., B. M., K. M., and W. H. analyzed the data. Y. M., K. M., and W. H. designed the study. A. K., K. U., Y. M., K. M., and W. H. wrote the manuscript.

Acknowledgments—We thank Ai Matsunami, Takuya Yokoyama, and Chizuru Tokunaga for excellent technical assistance. Diffraction data for crystal were collected at the BL38B1 station of SPring-8 (Hyogo, Japan) with the approval of JASRI (Projects 2015B2058, 2014B1137, 2014A1148, 2013B1260, and 2013A1106).

References

1. Davidson, A. L., Dassa, E., Orelle, C., and Chen, J. (2008) Structure, function, and evolution of bacterial ATP-binding cassette systems. *Microbiol. Mol. Biol. Rev.* **72,** 317–364, table of contents
2. Jones, P. M., and George, A. M. (2004) The ABC transporter structure and mechanism: perspectives on recent research. *Cell. Mol. Life Sci.* **61,** 682–699
3. Locher, K. P. (2009) Structure and mechanism of ATP-binding cassette transporters. *Philos. Trans. R. Soc. Lond. B Biol. Sci.* **364,** 239–245
4. Beis, K. (2015) Structural basis for the mechanism of ABC transporters. *Biochem. Soc. Trans.* **43,** 889–893
5. Oldham, M. L., Davidson, A. L., and Chen, J. (2008) Structural insights into ABC transporter mechanism. *Curr. Opin. Struct. Biol.* **18,** 726–733
6. Oldham, M. L., Chen, S., and Chen, J. (2013) Structural basis for substrate specificity in the *Escherichia coli* maltose transport system. *Proc. Natl. Acad. Sci. U.S.A.* **110,** 18132–18137
7. Locher, K. P., and Borths, E. (2004) ABC transporter architecture and mechanism: implications from the crystal structures of BtuCD and BtuF. *FEBS Lett.* **564,** 264–268
8. Gould, A. D., and Shilton, B. H. (2010) Studies of the maltose transport system reveal a mechanism for coupling ATP hydrolysis to substrate translocation without direct recognition of substrate. *J. Biol. Chem.* **285,** 11290–11296
9. Bao, H., Dalal, K., Cytrynbaum, E., and Duong, F. (2015) Sequential action of MalE and maltose allows coupling ATP hydrolysis to translocation in the $MalFGK_2$ transporter. *J. Biol. Chem.* **290,** 25452–25460
10. Hisano, T., Kimura, N., Hashimoto, W., and Murata, K. (1996) Pit structure on bacterial cell surface. *Biochem. Biophys. Res. Commun.* **220,** 979–982
11. Momma, K., Okamoto, M., Mishima, Y., Mori, S., Hashimoto, W., and Murata, K. (2000) A novel bacterial ATP-binding cassette transporter system that allows uptake of macromolecules. *J. Bacteriol.* **182,** 3998–4004
12. Hashimoto, W., Miyake, O., Momma, K., Kawai, S., and Murata, K. (2000) Molecular identification of oligoalginate lyase of *Sphingomonas* sp. strain A1 as one of the enzymes required for complete depolymerization of alginate. *J. Bacteriol.* **182,** 4572–4577
13. Hayashi, C., Takase, R., Momma, K., Maruyama, Y., Murata, K., and Hashimoto, W. (2014) Alginate-dependent gene expression mechanism in *Sphingomonas* sp. strain A1. *J. Bacteriol.* **196,** 2691–2700
14. Maruyama, Y., Itoh, T., Kaneko, A., Nishitani, Y., Mikami, B., Hashimoto, W., and Murata, K. (2015) Structure of a bacterial ABC transporter involved in the import of an acidic polysaccharide alginate. *Structure* **23,** 1643–1654
15. Nishitani, Y., Maruyama, Y., Itoh, T., Mikami, B., Hashimoto, W., and Murata, K. (2012) Recognition of heteropolysaccharide alginate by periplasmic solute-binding proteins of a bacterial ABC transporter. *Biochemistry* **51,** 3622–3633
16. Mishima, Y., Momma, K., Hashimoto, W., Mikami, B., and Murata, K. (2003) Crystal structure of AlgQ2, a macromolecule (alginate)-binding protein of *Sphingomonas* sp. A1, complexed with an alginate tetrasaccharide at 1.6-Å resolution. *J. Biol. Chem.* **278,** 6552–6559
17. Jackson, P. (1994) High-resolution polyacrylamide gel electrophoresis of fluorophore-labeled reducing saccharides. *Methods Enzymol.* **230,** 250–265
18. Momma, K., Mishima, Y., Hashimoto, W., Mikami, B., and Murata, K. (2005) Direct evidence for *Sphingomonas* sp. A1 periplasmic proteins as macromolecule-binding proteins associated with the ABC transporter: molecular insights into alginate transport in the periplasm. *Biochemistry* **44,** 5053–5064
19. Momma, K., Mikami, B., Mishima, Y., Hashimoto, W., and Murata, K. (2002) Crystal structure of AlgQ2, a macromolecule (alginate)-binding protein of *Sphingomonas* sp. A1 at 2.0 Å resolution. *J. Mol. Biol.* **316,** 1051–1059
20. Baba, S., Hoshino, T., Ito, L., and Kumasaka, T. (2013) Humidity control and hydrophilic glue coating applied to mounted protein crystals improves X-ray diffraction experiments. *Acta Crystallogr. D Biol. Crystallogr.* **69,** 1839–1849
21. Borths, E. L., Poolman, B., Hvorup, R. N., Locher, K. P., and Rees, D. C. (2005) *In vitro* functional characterization of BtuCD-F, the *Escherichia coli* ABC transporter for vitamin B12 uptake. *Biochemistry* **44,** 16301–16309
22. Otwinowski, Z., and Minor, W. (1997) Processing of X-ray diffraction data collected in oscillation mode. *Methods Enzymol.* **276,** 307–326
23. Vagin, A., and Teplyakov, A. (1997) *MOLREP*: an automated program for molecular replacement. *J. Appl. Crystallogr.* **30,** 1022–1025
24. Collaborative Computational Project, Number 4 (1994) The CCP4 suite: progarms for protein crystallography. *Acta Crystallogr. D Biol. Crystallogr.* **50,** 760–763
25. Murshudov, G. N., Vagin, A. A., and Dodson, E. J. (1997) Refinement of macromolecular structures by the maximum-likelihood method. *Acta Crystallogr. D Biol. Crystallogr.* **53,** 240–255
26. Adams, P. D., Afonine, P. V., Bunkoczi, G., Chen, V. B., Davis, I. W., Echols, N., Headd, J. J., Hung, L. W., Kapral, G. J., Grosse-Kunstleve, R. W., McCoy, A. J., Moriarty, N. W., Oeffner, R., Read, R. J., Richardson, D. C., *et al.* (2010) PHENIX: a comprehensive Python-based system for macromolecular structure solution. *Acta Crystallogr. D Biol. Crystallogr.* **66,** 213–221
27. Emsley, P., Lohkamp, B., Scott, W. G., and Cowtan, K. (2010) Features and development of Coot. *Acta Crystallogr. D Biol. Crystallogr.* **66,** 486–501
28. DeLano, W. L. (2010) *The PyMOL Molecular Graphics System*, version 1.3, Schrödinger, LLC, New York